1 Bulk Growth of Mercury Cadmium Telluride (MCT)

P. CAPPER

SELEX Galileo Infrared Ltd, Southampton, UK

1.1 INTRODUCTION

In the early days of mercury cadmium telluride (MCT) production (1960s and 1970s) bulk growth techniques were the predominant ones. As time progressed into the 1980s and 1990s various epitaxial techniques, particularly liquid phase epitaxy (LPE), metal-organic vapor phase epitaxy (MOVPE), and molecular beam epitaxy (MBE) took over MCT production, particularly for photovoltaic devices, due to their greater flexibility. However, in some centers bulk-growth developments continued and material grown by bulk-growth techniques is still used for first-generation photoconductive IR detectors and for optical components in IR applications. Because of the sensitive nature of the R&D work associated with the material the history of MCT is characterized by most centers developing their own routes somewhat independently of their international counterparts.

There are two main types of bulk growth technique; from the liquid and from the vapor; however, most work on MCT is from the liquid phase and vapor-phase growth is not discussed in this chapter. Of the many bulk growth techniques applied to MCT three are seen to dominate. These are solid state recrystallization (SSR), the traveling heater method (THM), and Bridgman/accelerated crucible rotation technique (ACRT). This chapter covers the major developments in these three techniques, but first the key area

Mercury Cadmium Telluride: Growth, Properties and Applications Edited by Peter Capper and James Garland

of phase equilibria is discussed. These equilibria are critical to establish the understanding and limitations of all growth techniques.

Central to the successful use of these materials are the dual issues of elemental purity and cleanliness in all stages of preparation and handling, particularly prior to high-temperature heat treatments. A wide variety of assessment techniques have also been developed to characterize the compositional, electrical, and structural properties as well as chemical purity, but these are covered in a separate chapter in this book (Chapter 16).

1.2 PHASE EQUILIBRIA

Two types of equilibria are of interest. One is the solid compound in equilibrium with the gaseous phase (vapor growth) and the other is solid–liquid–gaseous equilibria (growth from liquid/melt). These phase equilibria also help in understanding post-growth heat treatments, either during cool-down or during annealing processes to adjust the stoichiometry, and hence electrical properties of compounds. Solid–liquid–gaseous equilibria are described by three variables: temperature (T), pressure (P), and composition (x). It is, however, easier to understand the interrelations between these parameters by using two-dimensional projections such as T–x, P–T, and P–x plots.

A great deal of work has been carried out on the various phase equilibria ([1, 2] contain reviews in this area). The liquidus and solidus lines in the pseudobinary HgTe–CdTe system are shown in Figure 1.1 [1]. The wide separation between the liquidus and solidus, leading to marked segregation between CdTe and HgTe, influenced the development of all the bulk growth techniques. In addition to the solidus–liquidus separation high Hg

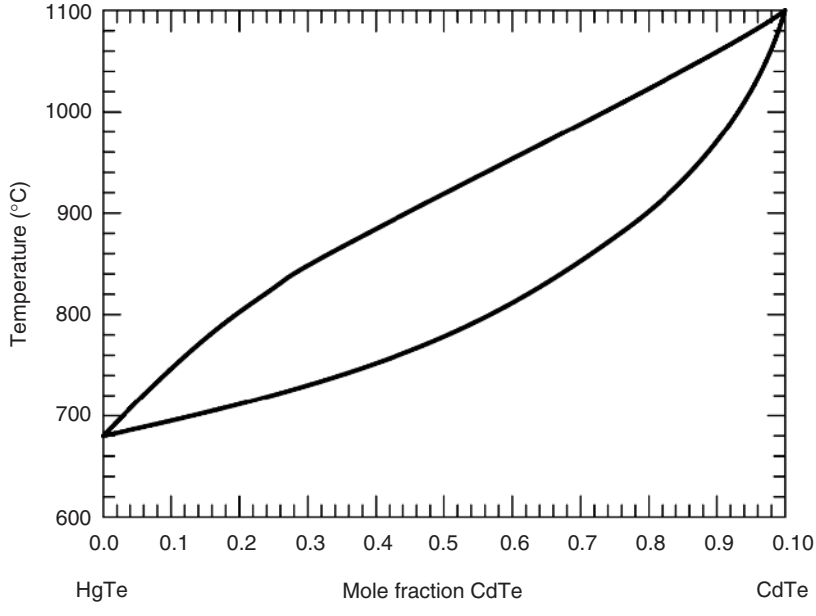

Figure 1.1 T–x phase diagram for the pseudo-binary CdTe-HgTe [1]. (Reprinted from EMIS Datareview Series No. 10, *Properties of Narrow-Gap Cadmium-Based Compounds*, ed. P. Capper, 56–58. Copyright (1994) IET)

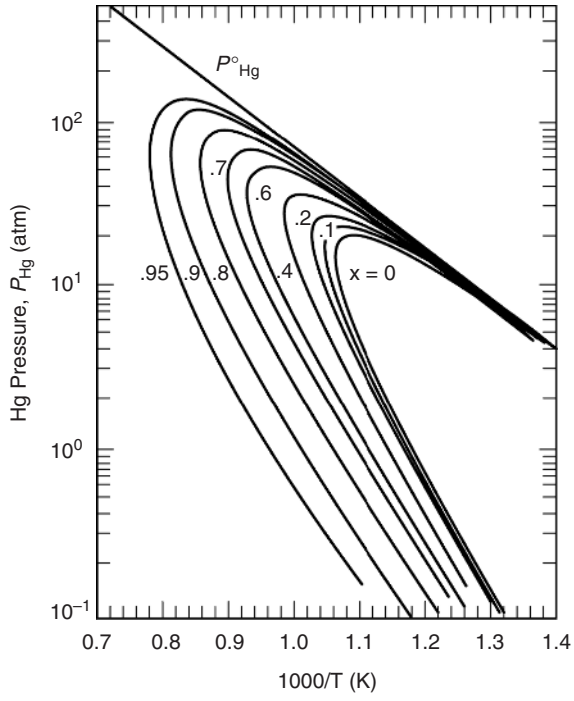

Figure 1.2 P–T diagram for $Hg_{1-x}Cd_xTe$ (MCT) [1]. (Reprinted from EMIS Datareview Series No. 10, *Properties of Narrow-Gap Cadmium-Based Compounds*, ed. P. Capper, 56–58. Copyright (1994) IET)

partial pressures are also influential both during growth and post-growth heat treatments. A full appreciation of the $P_{(Hg)}$–T diagram, shown in Figure 1.2, is therefore essential. Curves are the partial pressures of Hg along boundaries for solid solutions of composition x where the solid solution is in equilibrium with another condensed phase as well as the vapor phase. For example, for $x = 0.1$ and $10^3/\mathrm{T} = 1.3(\mathrm{K}^{-1})$ MCT exists for Hg pressures of 0.1 (Te-saturated) and 7.0 (Hg-saturated) atm.

1.3 CRYSTAL GROWTH

The vast majority of work on bulk growth of MCT has been from the melt. Several historical reviews have been published [3–8]. Micklethwaite [3] and Kruse [4] gave comprehensive information on the growth techniques used prior to 1980. Many techniques were tried in the early years but three prime techniques survived: SSR, THM, and Bridgman. Tennant *et al*. [9] provided an authoritative view of the then current major issues in growth techniques and noted that several countries still employed bulk-growth methods. They concluded that the electrical performance had only recently (at that time) been matched by LPE but pointed to the problems of structural defects and size limitations for use in second-generation infrared detectors. This chapter continues with reviews of the three basic bulk growth techniques, mainly using the more recent reviews of Tregilgas [10], Capper [7, 8], and Triboulet [11], although updates in these basic techniques are also given, where applicable.

1.3.1 Solid state recrystallization (SSR)

1.3.1.1 Introduction

Tregilgas [10] gave a detailed review of the SSR process and this section takes much of its content from that excellent review. Other names that have been used for this process are quench anneal (QA) and cast recrystallize anneal (CRA). Strictly speaking, SSR is crystal growth from the solid phase at temperatures close to the melting point. The technique was initially commercialized for the production of photoconductive detectors but was also used for second-generation focal plane arrays based on metal–insulator–semiconductor (MIS) detectors.

In the basic technique, pure elements are loaded into an etched silica ampoule (it is critical to avoid contact between the mercury and the cadmium during loading) and the charge is melted and rocked to ensure complete mixing. Charges are then normally quenched rapidly, into air or oil, to room temperature in either the vertical or near-horizontal orientation, see Figure 1.3. This produces a dendritic structure that is reduced/removed by the recrystallization step, which occurs at temperatures just below the solidus temperature for many days. Grain growth occurs and micro-inhomogeneities in composition are removed. A low-temperature annealing step, in the presence of mercury, is then used to convert the as-grown p-type material to n-type for subsequent use in detector fabrication. Many modifications were found necessary to reduce the defect densities to levels sufficient to make the MIS devices.

1.3.1.2 Growth

During compounding, mercury is lost from the melt to the vapor space above and results in excess tellurium in the quenched ingot. It is therefore desirable to control both the Hg

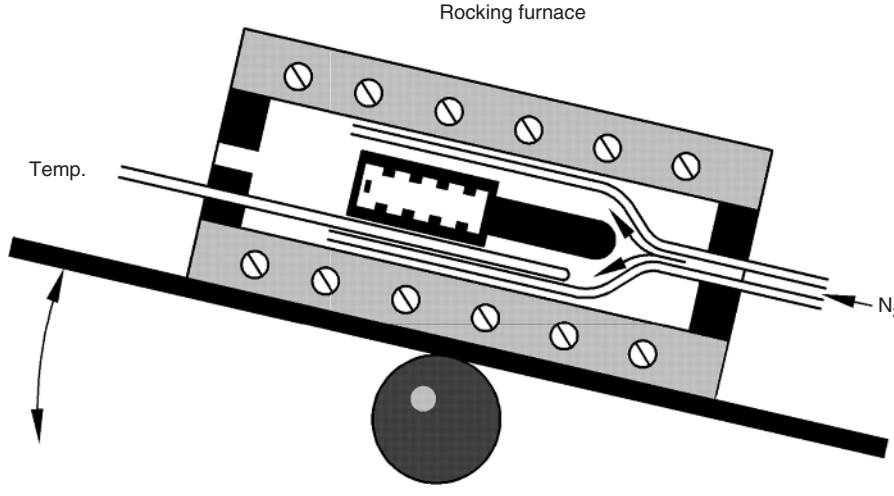

Figure 1.3 Schematic of rocking furnace with gas quenching tube [10]. (Reprinted with permission from *Progress in Crystal Growth and Characterization of Materials*, Developments in recrystallized bulk HgCdTe by J. H. Tregilgas, 28, 1-2, 57. Copyright (1994) Elsevier Ltd)

excess and the ampoule void space/seal-off length. Ingot diameters are limited by the burst pressures of the silica ampoules and the Hg vapor pressure (>40 atm) during elemental compounding. This necessitates thick-walled ampoules, but there are limits to this otherwise heat transfer during quenching is reduced and voids, holes and even "piping" can occur. For internal diameters of 8.0–12.5 mm wall thicknesses vary from 2 to 3 mm.

Compressed-gas cooling of the end of the ampoule is used to quench the ingot and the flow rate of this gas can be adjusted to vary the grain size and the dendrite arm spacing in the ingot, with 40–50 l min^{-1} being optimum. Figure 1.4 shows a typical as-quenched microstructure with dendrites and misfit dislocations. If quenching rates become too high then voids, shrinkage pipes, and/or compositional "coring" can all result [12, 13]. Subgrain boundaries result from the misalignments between the dendrite arms, and entrapped Te can also be present.

Following quenching the ingots are held near to the HgTe melting point for several days to allow homogenization of dendrites and grain growth to occur. The process that occurs during this step is one of secondary recrystallization, that is, grain growth, rather than primary recrystallization, that is, where new grains are nucleated and grow at the expense of older grains. On cooling following recrystallization Te often precipitates within the ingot, the extent of which is governed by the initial stoichiometry of the charge prior to cooling and by the Hg vapor pressure at the recrystallization temperature. Increasing the Hg partial pressure and slow cooling can be used to minimize Te precipitation.

Dislocation multiplication (up to 8–10 times higher) can result from the elimination of Te precipitates during this process step. This dislocation reduction anneal (DRA) process starts from the recrystallization temperature. Upon cooling, Te precipitation occurs. Re-encapsulation of the slices from such an ingot together with additional Hg is followed by re-heating and the excess Te is reduced by in-diffusing Hg. Upon subsequent cooling fewer Te precipitates form and the normal low-temperature type-conversion anneal

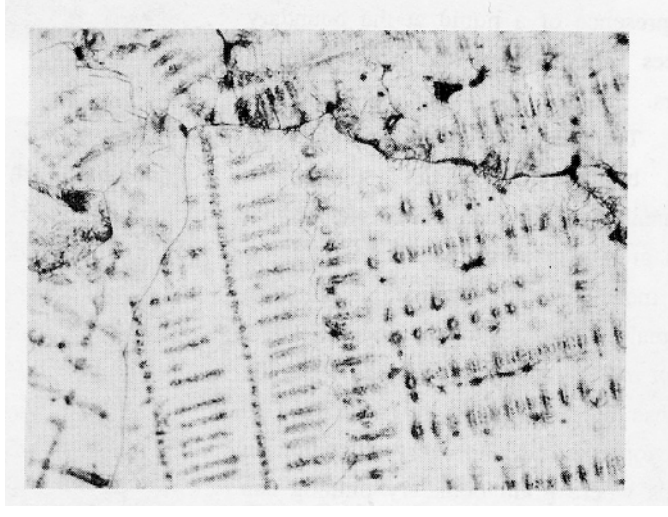

Figure 1.4 As-quenched microstructure showing dendrites and misfit dislocations [10]. (Reprinted with permission from *Progress in Crystal Growth and Characterization of Materials*, Developments in recrystallized bulk HgCdTe by J. H. Tregilgas, 28, 1-2, 57. Copyright (1994) Elsevier Ltd)

occurs without dislocation multiplication. Such a DRA step can lead to a net reduction in dislocation density of a factor of up to 100.

1.3.1.3 Characterization

After recrystallization the ingot is p-type due to a high metal vacancy concentration. The ingot is then sliced and the slices are annealed in Hg vapor to reduce Te precipitation and to fill the metal vacancies, leaving the material n-type, due, it is believed, to residual donor impurities. The temperatures are normally in the range of 200–300 °C and the anneal duration is selected to control the depth of the p/n junction, that is, the thickness of the n-type surface layer. Following annealing, Hall effect measurements are used to assess the carrier concentration and mobility of the material and hence its suitability for photoconductive device manufacture.

There are several sources of residual impurities in the final material. These include the raw elements, the silica ampoule, chemical etching of the elements and the silica ampoule, the loading environment, surface contaminants on slices after etching prior to annealing and the diffusion of fast-diffusing species, for example, Na and Cu, through the silica ampoule during low-temperature annealing.

Doping can be accomplished either by native defect control or deliberate addition of extrinsic impurities. By varying the Hg partial pressure during the low-temperature annealing step, for example, by adding Hg or using a vacuum, the material can be annealed under Hg-rich or Hg-deficient conditions, leading, respectively to n-type or p-type conduction. For extrinsic doping, noble metals such as Cu, Ag, and Au are preferred due to their ease of activation, also their distribution can be made homogeneous. Acceptor doping with Group V elements, for example, P, As, and Sb, shows inhomogeneous distributions that are difficult to homogenize due to the inherent low diffusion coefficients of these elements. In addition, Hg-rich annealing above 400 °C or the DRA process is necessary to activate these impurities. Doping with Cu at high levels was used successfully to manufacture MIS devices. Donor doping with In, Si, and I have all been accomplished. Donor doping using Al, Ga, In, and Br has also been accomplished by in-diffusion into slices, although high levels of In and Ga doping can be achieved by melt doping.

1.3.1.4 Variations on the basic technique

Alternatives to the basic SSR process have included “slush” growth [14], high-pressure growth [15], incremental quenching [16], and horizontal casting [17]. In the “slush” process the initial homogenous charge is held across the liquidus–solidus gap with the lower end solid and the upper end liquid. High-pressure growth (30 atm He gas) was used in an attempt to reduce structural defects by improved heat flow control and using intergranular Te as a moving liquid zone during the recrystallization step [15]. Incremental quenching involves extruding molten drops from an orifice onto a crucible base, and subsequently on the growing crystal [16]. The “slush” technique was used in production in the United States, until quite recently, while the incremental quenching technique has been used to provide large diameter feed material for THM growth [18]. Other developments have been made in the basic process [19, 20] but details available in the open literature are sketchy, due to proprietary constraints.

1.3.1.5 Summary

The SSR technique was used, predominantly in the United States, for first-generation photoconductive and second-generation MIS IR detectors. It has now largely been superseded by the various epitaxial techniques and is no longer actively researched, at least to this author's knowledge.

1.3.2 Traveling heater method (THM)

1.3.2.1 Introduction

Triboulet [11] gave a detailed review of the THM process and this section takes much of its content from that excellent review. Triboulet's premise for starting work on THM was that the alternative existing methods all suffered to varying degrees from the particulars of the HgTe–CdTe phase diagram, or required high pressures and/or their implementation could be complex. As a result of this crystals had limited compositional uniformity and/or restricted size. He concluded that what was needed was to achieve a growth process at lower temperatures, and hence lower pressures, reduced contamination, reduced defect levels and less departure from stoichiometry, that also led to a purification effect and ideally would facilitate seeding of growth. The THM method combines the purity advantages of zone refining and the low temperatures necessary to give large-area growth, uniform composition, low defects, and defined crystal orientation.

In essence, the method involves moving a molten zone through a solid homogeneous source material by slow movement of the ampoule relative to the heater, as shown in Figure 1.5. Matter is transported by convection and diffusion across the solvent zone in a

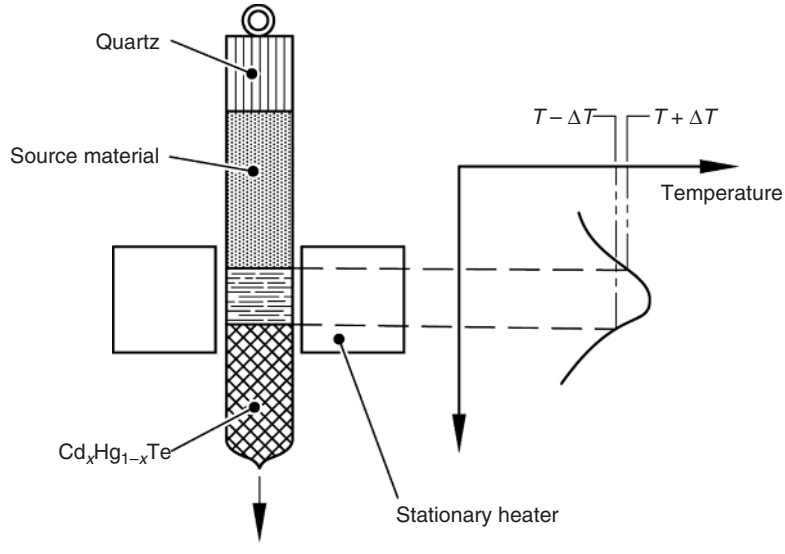

Figure 1.5 Principle of THM process [11]. (Reprinted with permission from *Progress in Crystal Growth and Characterization of Materials*, The Travelling Heater Method (THM) for $Hg_{1-x}Cd_xTe$ and related materials by R. Triboulet, 28, 1-2, 85. Copyright (1994) Elsevier Ltd)

temperature gradient that results from the ampoule movement. For alloys, a steady-state can be reached where the solvent zone dissolves a solid of composition C_0 at the upper hot interface then deposits, at near equilibrium, material of the same composition at the lower growth interface. The Te solution also serves to purify the material during the growth process. Seeding is relatively straightforward to arrange, leading to improved structure and orientation control. Finally, THM allows the growth of longer and larger-diameter material, up to 40 mm for MCT.

1.3.2.2 Growth

The required temperature profile must have a sharp temperature peak, producing a narrow molten zone (approximately the same dimension as the crystal diameter) and a high temperature gradient at the growth interface to prevent constitutional supercooling. A simple furnace arrangement was used successfully, in which an isothermal plane was arranged at the lower end of a nickel heating ring, that is, at the growth interface position. Thermal stability was found to be critical ($\pm 0.1\ ^\circ$C) to prevent the growth of parasitic nuclei.

Several solutions have been applied to the problem of producing suitable feed material. The most successful was that of using a cylindrical charge consisting of two segments, one CdTe and the other HgTe, with cross sections in a ratio corresponding to the desired alloy composition, which accomplished crystal diameters of up to 40 mm. As the ternary liquid solution cannot be in equilibrium with both binaries, and also because of the high Hg pressures, coring can occur at the Hg-dissolving interface, which is moved to a lower temperature than that of the CdTe, leading to small composition fluctuations.

1.3.2.3 Characterization

Using Te as the solvent steady-state growth is attained asymptotically after an initial transient, providing the source material is macroscopically homogeneous and the temperature and travelling rate of the solvent zone are constant. Very slow growth rates (0.1 mm h^{-1}) are typical [5]. Figure 1.6 shows a typical axial composition profile of a MCT ingot. The initial transient causes the x value to decrease from its original value to the desired $x \sim 0.2$ region over $\sim$2 cm. To avoid the initial transient in the growth the solvent-zone composition was adjusted to yield the desired composition from the start of growth. The required composition is determined from the Te-rich corner of the HgCdTe phase diagram, and is found to depend on the growth temperature and the temperature gradient (and hence the travelling rate).

There is a marked purification effect produced by solution zone refining, particularly when Te is used. The segregation of many impurities has been shown to be higher in liquid Te than in liquid CdTe. A doping experiment, using gold, showed the marked purification obtained in THM growth. A segregation coefficient of 0.003 was obtained, compared with $\sim$0.03 from Bridgman/ACRT [5]. Low impurity levels were found from mass spectrometry measurements and the background donor levels were also low, indicating high purity.

Donor doping has been achieved by using an In-doped CdTe crystal and an undoped HgTe crystal as the starting materials.

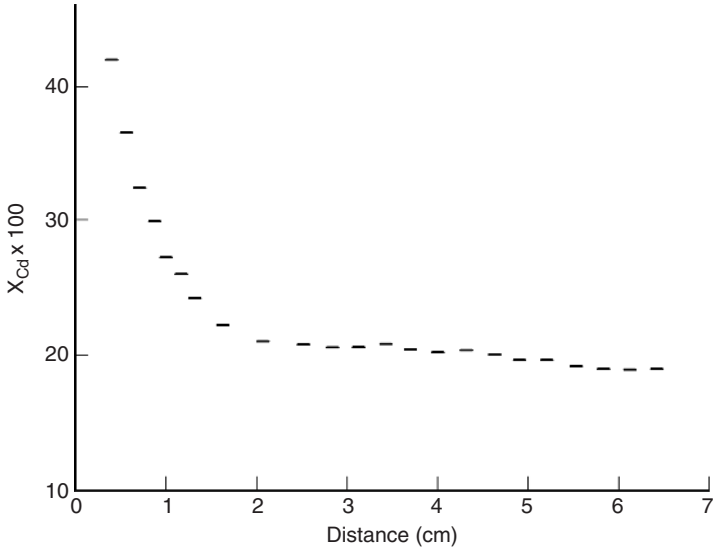

Figure 1.6 Compositional profile of THM MCT crystal using Te as solvent, for $x = 0.2$ [11]. (Reprinted with permission from *Progress in Crystal Growth and Characterization of Materials*, The Travelling Heater Method (THM) for $Hg_{1-x}Cd_xTe$ and related materials by R. Triboulet, 28, 1-2, 85. Copyright (1994) Elsevier Ltd)

Natural convection is expected to be the dominant mechanism of mass transport in THM. This made it sensible to add ACRT to the THM process and a "saw-tooth" variation of rotation rate was used. A significant improvement in both radial and axial compositional homogeneity was obtained. ACRT also allowed higher growth rates, up to 8.5 mm day^{-1}, to be obtained [21].

A more recent report [22] showed how a rotating magnetic field can be used to control heat and mass transport. Crystals were 25 mm in diameter, 60 mm long, and were grown at a rate of 2.5 μm min^{-1}. Magnetic fields of 2–6 mT were used and growth periods were up to 200 h. For the crystal grown with a 2-mT magnetic field the radial composition uniformity was seen to be 0.003–0.007 in x. After low-temperature Hg annealing the material was n-type with carrier concentration $\sim 1 \times 10^{15}$ and mobility $\sim 1 \times 10^5$ cm^2/V s, demonstrating the high purity of the material.

Oriented seed crystals of CdTe were used to produce MCT crystals up to 30 mm diameter in both [111] and [100] orientations. Without seeding crystals usually consist of some large grains, the lower the Cd content the larger the grains. A flat or convex interface is crucial to producing crystals with fewer extended defects, a low-temperature gradient at the interface also helps.

Higher etch pit densities (dislocations) and small twins are observed at the periphery of slices. Secondary nucleation at the ampoule walls, resulting from the local concavity of the growth interface, is the probable cause of the twins. These types of defects and subgrain densities become progressively more common toward the tail-end of THM crystals. However, careful control of the interface shape, low-temperature gradients, low temperatures, and suppression of constitutional supercooling can lead to subgrain-free material.

As-grown material shows a conductivity type that is controlled by the growth temperature. This is understandable based on phase equilibria diagrams, the higher the growth

temperature the more nearly stoichiometric the material. Experimental results for $x = 0.22$ showed the material to be p-type for a growth temperature of 600 °C and n-type for 700 °C, under otherwise identical growth conditions. For as-grown p-type material low-temperature annealing in Hg vapor has been shown to lead to n-type conductivity, proving that deviations from stoichiometry, that is, metal vacancies, are responsible for the p-type conductivity. Carrier concentrations of 2–5 $\times$ 10^{14} cm^{-3} with mobilities of 1.6 $\times$ 10^5 to 5 $\times$ 10^4 $cm^2/V\,s$ were found for $x = 0.2$ and 0.3 material, together with high minority carrier lifetimes of 3 and 30 μs, respectively. These data indicate highly pure material.

1.3.2.4 Summary

THM was developed predominantly in France, and has produced some of the largest, highest-purity MCT crystals. Both photoconductive and photovoltaic detectors, the latter out to telecommunications wavelengths of 1.3 μm, have been made in this material. Work on this technique though has now probably ceased, again to the best of this author's knowledge.

1.3.3 Bridgman

1.3.3.1 Introduction

Historically, the first technique used in the United Kingdom was the Bridgman process. In about 1980, the ACRT was developed as a modification of the Bridgman process. The following sections give details of these two growth techniques. Reviews of bulk growth can be found in [7, 8, 23].

Two fundamentally different approaches were initially followed to improve the basic Bridgman process, based on control of melt mixing and of heat flows, respectively. The former has been studied by this author and coworkers [24, 26, 28] while the latter includes the work of Szofran and Lehoczky [25], among others. In the Bridgman process, elemental Cd, Hg, and Te are loaded into a clean silica ampoule, homogenized by melting/rocking and then frozen slowly from one end in a vertical system to produce, normally, a large-grained ingot. Marked segregation of CdTe with respect to HgTe occurs in the axial direction, but this leads to an advantage of the Bridgman process over other techniques, that is, material in both ranges of interest ($x = 0.3$ and 0.2, for 3–5 and 8–12 μm, respectively) is produced in a single run.

1.3.3.2 Elemental purification (mercury and tellurium)

All bulk growth processes for MCT use pure elements as the starting materials and silica ampoules. Despite this, experience at this author's laboratory has shown that problems can occur using bought-in elements directly. These problems manifest themselves as charges sticking to silica ampoules, believed to be due to oxygen on Te and/or Cd surfaces, or as high background donor levels in the resulting MCT. For these reasons, and to maintain a consistent and controlled product, purification of both Te and Hg just prior to use takes place.

Bought-in Hg, in triple-distilled form, is passed through a sub-boiling point vacuum distillation process in a high-purity, all-silica apparatus. The amounts of Cu and/or Ag (both acceptors in MCT) are significantly reduced by this process and possibly other elements also. Tellurium purification is by zone refining in flowing hydrogen at ~500 °C. Molten zones are traversed down the boat and this has the effect of moving impurity elements with segregation coefficients, k, of <1 to the tail of the bar while those with $k > 1$ segregate to the tip of the bar. On removal, the tip and tail sections are discarded, while the central section (~4 kg) is ready for use with no further chemical cleaning necessary.

1.3.3.3 Growth and characterization

Elemental Cd (unetched), plus in-house purified Hg and Te are loaded, in a nitrogen-purged glove box into an etched, washed, heavy-wall (3 mm) silica ampoule (diameter 12–13 mm). A start composition of $x = 0.12$ is used and homogenization is by melting/rocking. Charges are placed in a vertical grower, re-melted, and then frozen slowly (0.5 mm h^{-1}) from one end in a vertical system to produce a large-grained ingot. Each growth unit is housed in a semi-sealed cell to manage the occasional explosions resulting from the ~70 atm pressure caused by the free Hg. Slow rotation about the vertical axis is used to reduce radial temperature variations. Slices cut from the resulting crystals are assessed for x uniformity with infrared transmission (IRT) measurements and Hall measurements at 77 K for the electrical parameters.

Photoconductive devices require low carrier concentration n-type material and this was produced by improving the purity of the starting materials. Low n-type levels ($\ll 1 \times 10^{15}$ cm^{-3}) were achieved in the as-grown state for x = 0.2–0.3, an obvious advantage in terms of reduced handling for Bridgman growth as no annealing stage was required – unlike other bulk methods. Bridgman material was used [29] to establish the pressure–temperature diagram, by a combination of isothermal and two-temperature annealing. On the Hg-rich side at temperatures below 320 °C the n-type carrier concentration is controlled by residual impurities. The p → n conversion is due to Hg filling metal vacancies. Conversion from n → p was achieved by two-temperature annealing with the Hg at a lower temperature than the MCT, in order to introduce metal vacancies.

Most impurity elements are electrically active in accordance with their position in the periodic table [30]. This behavior is linked to the stoichiometry at growth, that is, those elements that substitute on Te lattice sites have to be forced onto the correct sites in Te-rich material. Group I and III elements are acceptors and donors, respectively, on the metal sites. There is evidence, however, that some Group I elements can migrate at low temperatures to grain boundaries or to the surface of samples. Bridgman benefits from marked segregation of impurities due to its slow growth rate, leading to very low levels of impurities.

1.3.4 Accelerated crucible rotation technique (ACRT)

Limits on controlling melt mixing in the Bridgman process necessitated a means of stirring melts contained in sealed, pressurized ampoules. The ACRT of Scheel [31] was utilized and the first report was given in [32]. These effects were developed and discussed in more detail in several later papers (see [8] for a review) and are briefly outlined here.

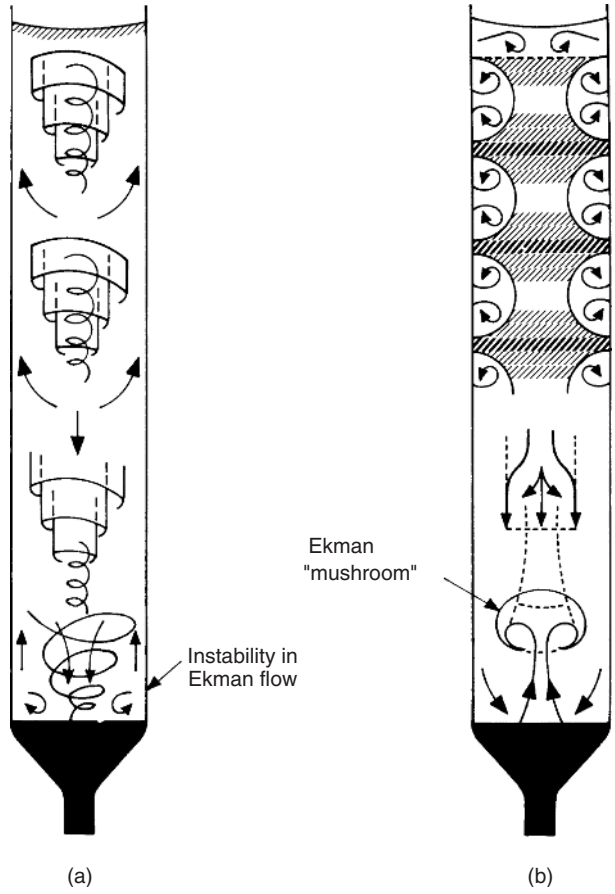

Figure 1.7 Flows in a flat-based container during ACRT: (a) spin-up and (b) spin-down [8]. (Reprinted with permission from *Progress in Crystal Growth and Characterization of Materials*, The role of accelerated crucible rotation in the growth of $Hg_{1-x}Cd_xTe$ and CdTe/CdZnTe by P. Capper, 28, 1-2, 1. Copyright (1994) Elsevier Ltd)

Figure 1.7 depicts the flows as seen in water simulation trials. All three predicted flow patterns were seen and the most vigorous stirring arose due to Ekman flow for distances of the radius, R, to $2R$ from the container base (Ekman volume), particularly when a flat-based container was used. Brice *et al*. [33] reviewed the models developed for flows induced by ACRT and summarized by identifying three distinct flow regimes as the acceleration/deceleration rate increases. For small accelerations, axially symmetric fluid flows increase the symmetry of heat and mass flows. Moderate accelerations produce axial and radial fluid flows at the base of the column ($R-2R$) that stir the fluid in this region only. Large accelerations give rise to unstable asymmetric flows. The system is characterized by the Reynolds number and Brice *et al*. [33] list the critical Reynolds numbers and the corresponding rotation rates for the parameters typical of MCT melts.

Various rotation sequences and start compositions were investigated and $x = 0.19$ was chosen as the preferred start composition. For these crystals grown with short run and

stop times (8 s, 1 s) there was a region (several centimeters long) of $x = 0.21$ material with axial and radial x uniformity of ± 0.002, thus ACRT gives a 5- to 10-fold increase in potentially usable material. Radial x variations were ± 0.002 at all wavelengths (i.e., $0.19 < x < 0.34$), demonstrating the reproducibility of the process and suggesting that relatively flat interfaces are present throughout the growth process. Increasing the maximum ACRT rotation rate eventually increased the interface depths and the preferred region was seen to be from 25 to 60 rpm, for a 13-mm diameter crystal. Because of the small radial variations in composition growth of larger-diameter crystals (up to 20 mm) was also possible using ACRT and the radial variation in wavelength for a 20-mm diameter slice from a crystal grown with a maximum rotation rate of 25 rpm was ~ 0.1 μm.

Recently, work was undertaken in the author's laboratory to extend the ACRT process to produce near-IR material, using higher starting x values [35] and larger-diameter material was grown. An improved ampoule seal-off procedure was developed to enable growth at the higher temperatures (hence higher pressures) needed for these higher-x start crystals.

Figure 1.1 shows the pseudo-binary phase diagram of the HgTe–CdTe system. The initial goal was to produce material of $x > 0.7$, that is, <1.4 μm cutoff wavelength. Figure 1.1 shows that this necessitates using starting x values of 0.33–0.35. Figure 1.2 shows the pressure–temperature phase diagram for various x values. This amply demonstrates how the maximum growth temperature and hence the Hg vapor pressure increases as x increases. Standard bidirectional rotation ACRT was employed with rapid acceleration/deceleration (in 1–2 s) with maximum rotation rates of 25–30 rpm. Figure 1.8 shows the excellent radial uniformity in wavelength obtained in these high-x start crystals. This slice has an average wavelength of ~ 0.91 μm ($x \sim 0.93$), the shortest wavelength MCT slice recorded so far from a bulk-grown crystal. A new assessment tool now used for these high-x crystals is that of IR imaging. By placing a black body on one side of the slice (polished on both sides to ~ 1 mm thickness) and a medium wavelength (MW) camera system on the other, images can be taken that show up IR-absorbing defects. This is a rapid, noncontact assessment method that can be used for all slices with cutoff wavelengths less than that of the camera system's detector. Figure 1.8 shows that the ~ 0.91-μm

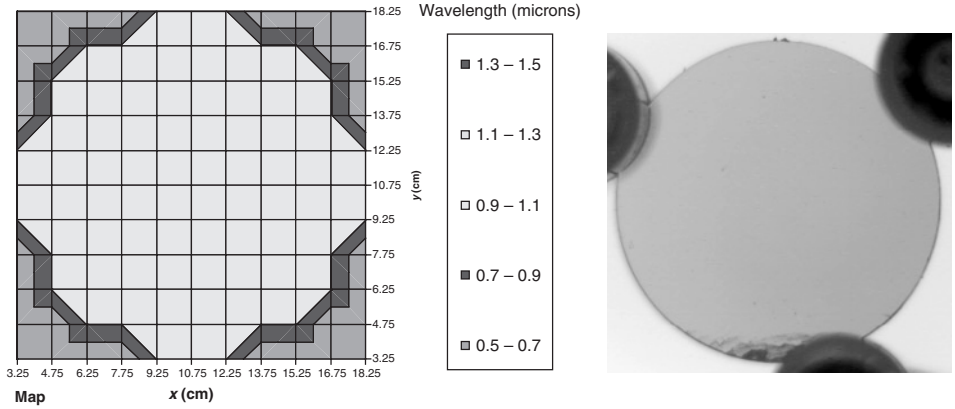

Figure 1.8 Radial distribution of wavelength (in μm at room temperature -0.91 μm $\equiv x \sim 0.93$) in a 20-mm diameter slice. (See Plate 1)

slice had excellent transmission properties with no grain boundaries or Te precipitates, unlike in earlier crystals at longer wavelengths.

A second aim of this work was to scale-up growth, using ACRT to maintain x uniformity. Several 40-, 50-, and 70-mm diameter crystals have been grown, despite no increase in the ampoule wall thickness! Figure 1.9 shows slices from 20-, 40-, 50-, and 70-mm diameter crystals. The 70-mm crystal is the largest diameter crystal grown anywhere, to this author's knowledge. In tandem with increasing diameter the weight of crystals was also increased, to maintain the number of usable slices. The largest weight currently used for 50-mm diameter crystals is ~2 kg. The highest x value seen in these 50-mm crystals (from a 30% start) is ~1.5 μm ($x \sim 0.67$) and Figure 1.10 shows the wavelength uniformity of this slice, together with the IR image of the adjacent slice, where a central area (~36 × 36 mm in size) can be seen to be clear of defects or grain boundaries.

The electrical properties of ACRT material differ from those of equivalent Bridgman crystals [30]. Material with $x > 0.3$ is n-type as-grown, at a level above that found for Bridgman crystals but, at $x < 0.3$, the material is p-type. Such material converts to low ($<1 \times 10^{15}$ cm^{-3}) n-type on the standard anneal treatment [29] indicating that metal vacancies are the cause of the p-type behavior. Groups I and III elements are acceptors

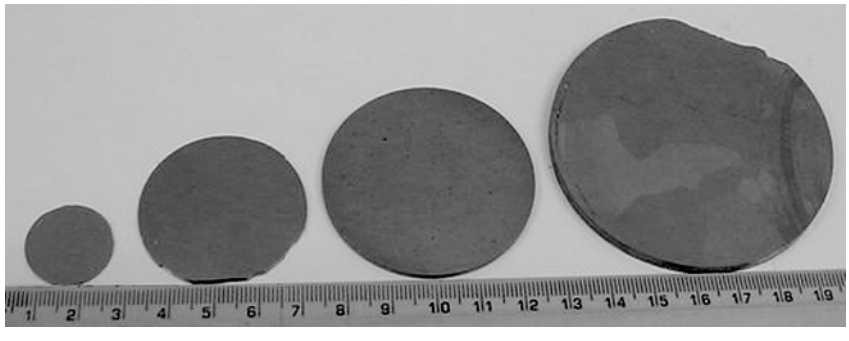

Figure 1.9 Comparison of 20-, 40-, 50-, and 70-mm MCT slices

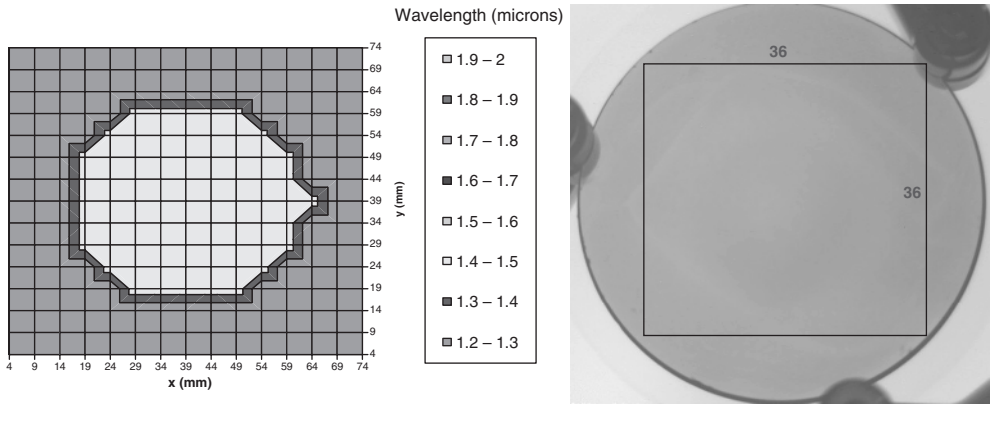

Figure 1.10 Radial distribution of wavelength (in μm at room temperature) in 50-mm diameter high-x slice from 30% start. (See Plate 2)

and donors, respectively, on the metal sites as they are in Bridgman. Groups V and VII are inactive dopants in those portions of ACRT crystals that are Te-rich as-grown, that is, $x < 0.3$, but are active dopants for $x > 0.3$ where metal-rich conditions prevail, as found in Bridgman material. In general, impurity segregation coefficients decrease in ACRT crystals, when compared to standard Bridgman [8, 34, 36].

1.3.4.1 Uses in IR devices

The low n-type carrier levels and high lifetime of Bridgman/ACRT material is well suited to give high-performance signal processing in the element (SPRITE) detectors [37]. In a study of far-IR detection at 350–1200 μm, Kimmitt *et al*. [38] found that ACRT MCT ($0.39 < x < 0.53$ and 3×10^{13} to 2×10^{14} cm^{-3} n-type) acted as an impurity photoconductor. Charlton *et al*. [39] listed the various space applications that used bulk material to make discrete IR detectors, both photoconductive and photovoltaic. Ashley *et al*. [40] demonstrated room-temperature operation in photoconductors made in ACRT-grown material. There are some 5000–6000 UK common module imagers in service worldwide that are based on this bulk material. This bulk material is still used at Selex Galileo Infrared Ltd for photoconductive arrays of IR detectors, including SPRITEs.

The first staring array imagery in the 8–14 μm band (77 K) was demonstrated [41] using ACRT MCT as the detector material. Ballingall *et al*. [42] discussed the effects of major grain boundaries on two-dimensional array performance, and Baker *et al*. [43] reported that such structure leads to anomalous crosstalk between adjacent diodes. Despite the potentially damaging subgrains, a 32×32 array (4.5 μm cutoff) with only a single defective element was made in ACRT material. Both 3–5 and 8–14 μm band arrays of 64×64 elements were made in ACRT material [43]. Yields of these larger arrays, however, were low due to the subgrain structure, hence the movement towards using epitaxial material.

1.3.4.2 Other developments

Hoschl *et al*. [27] developed a modified Bridgman process in which a melt of constant composition is arranged above the growing crystal. As growth proceeds the CdTe removed by the crystal growth is replaced above the melt by a piece of CdTe floating on the melt surface. Normally single crystals were obtained. The radial x variations, determined by electron-probe microanalysis was estimated as ± 0.005, being higher at the edge of slices, as in normal Bridgman. Diodes made in this material were comparable to those made in THM material. The disadvantages of the technique include the long growth time, two to three months, and the inferior compositional uniformity, compared to ACRT [27]. However, it is a simpler process in that it only requires binary compounds to be formed initially, and it produces material of equivalent purity to THM and ACRT.

In a series of recent papers [44–48], this material has been used to study various effects of p–n junction formation and also to study some of the fundamental properties of the material. The latter have included minority carrier diffusion lengths and lifetimes [44], galvanomagnetic and thermoelectric parameters [45], and native point defects [46]. Reference [47] showed the temperature dependence of the depth of p to n conversion during argon milling. Reference [46] interpreted changes in electrical conductivity with time after

reactive ion etching in terms of release and diffusion of Hg interstitials with a diffusion coefficient of $>10^8$ cm^2 s^{-1}.

A recent report has been made of a new method of producing MCT crystals using a high-pressure Bridgman process [49]. In this technique two stages are used to produce the starting material. In the first stage the composition is fixed at 0.04–0.06. This is melted, at a relatively low temperature, and then a second charge with a composition of ~0.4 is loaded on top of the initial charge. Crystal growth then takes place at a slow rate of ~0.21 mm h^{-1} in a low-temperature gradient (5 °C cm^{-1}) at a low growth temperature of ~710 °C. Crystals up to 40 mm in diameter have been produced and the uniformity of composition in the axial direction, albeit only from density measurements that give an average figure, is claimed to be good. Uniformity in the radial direction is quoted as ±0.001 in composition, again albeit over only the central 6 × 6 mm area. No electrical data were given.

1.3.4.3 Summary

In the Bridgman growth of MCT, a controlled increase in melt mixing, produced by ACRT, leads to an improvement in radial compositional variations and good axial uniformity resulting in a factor of 10 increase in overall material yield over normal Bridgman growth. Large-diameter crystals (13–20 mm) have been grown with a high degree of radial x uniformity by ACRT. Electrical and chemical characterization shows that high-purity material is obtained (when pure elements are used) and this allows the manufacture of a wide variety of high-performance photoconductive IR detectors. Bulk growth techniques for MCT are still in production and continue to satisfy the needs of the first-generation IR detectors, based on photoconductors, for both military and commercial use. The use of ACRT also made possible the fabrication of early two-dimensional arrays of photodiodes with a high degree of uniformity of response. This type of material has also been used to demonstrate non-equilibrium detector operation. Grain structure prevents it from being useful in larger-area detector arrays. Recently, larger-diameter crystals, up to 70 mm, have been grown in the author's lab, which are aimed at optical component applications rather than IR detectors. In addition, higher-x samples are being produced, currently up to $x \sim 0.9$ in 20-mm diameter crystals.

Other, notably the Czech and Chinese, groups have developed modifications to the basic Bridgman process that produce usable material. The former group use a piece of CdTe floating on the melt to act as the replenishment source, while the latter group use a two-stage process to achieve the same effect, that is, to replenish the CdTe taken out of the melt during crystal growth. IR devices have been made in the material of the former group but it is still too early to tell if the Chinese technique will produce suitable material for device fabrication.

1.4 CONCLUSIONS

Despite the use of the various epitaxial growth techniques to produce MCT material for second- and third-generation IR devices, bulk-grown material continues to be used for some first-generation photoconductive devices and for some optical components. This chapter summarizes the three main techniques used to produce bulk MCT material,

namely, SSR, THM, Bridgman and their variants. This material was mainly used for first-generation photoconductive IR detectors, although the first small focal plane arrays, that is, second-generation devices were also made in bulk material. All three techniques have their advantages and disadvantages, which have been outlined above. Currently, it is thought that only material grown by modifications of the Bridgman process is being actively researched. It will probably be several more years before bulk material is made completely redundant by epitaxial processes.

REFERENCES

[1] Brebrick, R.F. (1994) in *Properties of Narrow Gap Cadmium-based Compounds*, EMIS Datareview Series No. 10 (ed. P. Capper), IEE, London, p. 55.
[2] Brice, J.C. (1986) *Prog. Cryst. Growth Charact.*, **13**, 39.
[3] Micklethwaite, W.F.H. (1981) *Semicond. Semimet.*, **18**, 9.
[4] Kruse, P.W. (1981) *Semicond. Semimet.*, **18**, 1.
[5] Triboulet, R., Nguyen Duy, T., and Durand, A. (1985) *J. Vac. Sci. Technol. A*, **3**, 95.
[6] Maier, H. (1988) N.A.T.O. Advanced Research Workshop on the Future of Small-gap II-VI Semiconductors, Liege, Belgium.
[7] Capper, P. (1994) in *Properties of Narrow Gap Cadmium-based Compounds*, EMIS Datareview Series No. 10 (ed. P. Capper), IEE, London, p. 55.
[8] Capper, P. (1994) *Prog. Cryst. Growth Charact.*, **28**, 1.
[9] Tennant, W.E., Cockrum, C.A., Gilpin, J.B. *et al*. (1992) *J. Vac. Sci. Technol. B*, **10**, 1359.
[10] Tregilgas, J.H. (1994) *Prog. Cryst. Growth Charact.*, **28**, 57.
[11] Triboulet, R. (1994) *Prog. Cryst. Growth Charact.*, **28**, 85.
[12] Bartlett, B.E., Capper, P., Harris, J.E., and Quelch, M.J.T. (1979) *J. Cryst. Growth*, **47**, 341.
[13] Vydyanath, H.R. (1996) *J. Cryst. Growth*, **161**, 64.
[14] Harman, T.C. (1972) *J. Electron. Mater.*, **1**, 230.
[15] Vere, A.W., Straughan, B.W., Williams, D.J. *et al*. (1982) *J. Cryst. Growth*, **59**, 121.
[16] Colombo, L., Syllaios, A.J., Perlaky, R.W., and Brau, M.J. (1985) *J. Vac. Sci. Technol. A*, **3**, 100.
[17] Sharma, R.K., Singh, V.K., Mayyar, N.K. *et al*. (1987) *J. Cryst. Growth*, **131**, 565.
[18] Colombo, L., Chang, R.R., Chang, C.J., and Baird, B.A. (1988) *J. Vac. Sci. Technol. A*, **6**, 2795.
[19] Ziegler, J. (1986) US Patent 4, 591,410.
[20] Higgins, W.M., Pultz, G.N., Roy, R.G., and Lancaster, R.A. (1989) *J. Vac. Sci. Technol. A*, **7**, 271.
[21] Bloedner, R.U. and Gille, P. (1993) *J. Cryst. Growth*, **130**, 181.
[22] Senchenkov, A.S., Barmin, I.V., Tomsa, A.S., and Krapukhin, V.V. (1999) *J. Cryst. Growth*, **179**, 552.
[23] Capper, P. (1987) in *Properties of Mercury Cadmium Telluride*, EMIS Datareview Series No. 10 (eds J.C. Brice and P. Capper), IEE, London.
[24] Capper, P. (1989) *Prog. Cryst. Growth Charact.*, **19**, 259.
[25] Szofran, F.R. and Lehoczky, S.L. (1984) *J. Cryst. Growth*, **70**, 349.
[26] Bittner, H., Hoschl, P., and Schubert, B. (1991) *Cryst. Res. Tech.*, **26**, 667.
[27] Hoschl, P., Grill, R., Svoboda, J. *et al*. (1994) *J. Cryst. Growth*, **138**, 956.
[28] Capper, P., Harris, J.E., Nicholson, D., and Cole, D. (1979) *J. Cryst. Growth*, **46**, 575.
[29] Jones, C.L., Quelch, M.J.T., Capper, P., and Gosney, J.J.G. (1982) *J. Appl. Phys.*, **53**, 9080.
[30] Capper, P. (1991) *J. Vac. Sci. Technol. B*, **9**, 1667.
[31] Scheel, H.J. (1972) *J. Cryst. Growth*, **13/14**, 560.
[32] Capper, P. and Gosney, J.J.G. (1981) U.K. Patent 8, 115,911.

[33] Brice, J.C., Capper, P., Jones, C.L., and Gosney, J.J.G. (1986) *Prog. Cryst. Growth Charact.*, **13**, 197.
[34] Jungcheng, L., Wanqu, J., and Yaohe, Z. (1997) *Prog. Nat. Sci.*, **7/2**, 215.
[35] Capper, P., Maxey, C.D., Butler, C. *et al*. (2004) *J. Mater. Sci.: Mater. Electron.* **15**, 721.
[36] Capper, P. (2002) *J. Mater. Sci.: Mater. Electron.*, **12/8**, 423.
[37] Elliott, C.T. (1994) in *Properties of Narrow Gap Cadmium-based Compounds*, EMIS Datareview Series No. 10 (ed. P. Capper), IEE, London, p. 311.
[38] Kimmitt, M.F., Lopez, G.C., Giles, J.C. *et al*. (1985) *Infrared Phys.*, **25**, 767.
[39] Charlton, D.E., Moore, L.G., and McMillan, W.I. (1992) *Proceedings of the ESA Symposium on Photon Detectors for Instrumentation*, ESTEC, Noordwijk.
[40] Ashley, T., Elliott, C.T., and Harker, A. (1986) *Infrared Phys.*, **26**, 303.
[41] Ballingall, R.A. (1981) *Conference on Advanced IR Detectors and Systems*, IEE, London, p. 70.
[42] Ballingall, R.A., Blenkinsop, I.D., Lees, D.J. *et al*. (1983) *Conference on Advanced IR Detectors and Systems*, IEE, London, p. 6.
[43] Baker, I.M., Parsons, J.E., Lewis, J.H.W. *et al*. (1985) *Proc. SPIE*, **588**, 16.
[44] Franc, J., Belas, E., Toth, A.L. *et al*. (1999) *J. Cryst. Growth*, **197**, 593.
[45] Moravec, P., Grill, R., Franc, J. *et al*. (2001) *Semicond. Sci. Technol.*, **16**, 7.
[46] Belas, E., Grill, R., Franc, J. *et al*. (2001) *J. Cryst. Growth*, **224**, 52.
[47] Belas, E., Grill, R., Franc, J. *et al*. (1996) *J. Cryst. Growth*, **159**, 1117.
[48] Belas, E., Franc, J., Toth, A.L. *et al*. (1996) *Semicond. Sci. Technol.*, **11**, 1116.
[49] Wang, Y., Li, Q., Han, Q. *et al*. (2010) *J. Cryst. Growth* (in press).